A&A 461, 1127–1132 (2007)
DOI: 10.1051/0004-6361:20053736

Astronomy & Astrophysics

Excitation of electrostatic fluctuations by jets in a flaring plasma

R. Miteva, G. Mann, C. Vocks, and H. Aurass

Astrophysikalisches Institut Potsdam, An der Sternwarte 16, 14482 Potsdam, Germany
e-mail: rmiteva@aip.de

Received 30 June 2005 / Accepted 6 September 2006

ABSTRACT

Context. During magnetic reconnection as the proposed basic process of solar flares, hot high speed plasma streams (jets) are ejected from the reconnection site. Jets are sometimes associated with type III radio bursts as signatures of electron beams in the solar corona.
Aims. The interaction of such a jet with the surrounding coronal plasma is investigated concerning the generation of electrostatic fluctuations.
Methods. The conditions of excitations of such waves are studied in detail under coronal conditions by solving the linearized Vlasov-Maxwell equations.
Results. The interaction of a jet with the background plasma leads to an instability for a small range of jet speeds exciting electrostatic waves in the sense of the ion-acoustic mode. Electrons can be energized by their interaction with these electrostatic fluctuations. Such energetic electrons can be the source of type III radio bursts and/or non-thermal X-ray radiation as observed during solar flares.

Key words. waves – instabilities – acceleration of particles – Sun: flares – Sun: radio radiation

1. Introduction

During solar flares stored magnetic field energy is suddenly released and transferred into plasma heating, mass motions (e.g., jets and/or coronal mass ejections), energetic particles (e.g., electrons, protons, and heavy ions), and radiation across the whole electromagnetic spectrum, i.e., from radio waves up to γ-rays (Heyvaerts 1981). It is commonly accepted that the process of magnetic reconnection is responsible for this happening. If two magnetic field lines with opposite directions approach each other due to their photospheric footpoint motion, a current sheet is established between them (see Fig. 1). If the electric current exceeds a certain critical value, the anomalous resistivity is suddenly increased by exciting plasma waves owing to various plasma instabilities (see, e.g., Treumann & Baumjohann 1997). That leads to the onset of magnetic reconnection. Due to the strong curvature of the magnetic field lines after their reconnection, the plasma is shooting away from the reconnection site leading to the establishment of (sometimes oppositely directed) jets of hot plasma (see Fig. 1). As already discussed by Yokoyama & Shibata (1994, 1995), magnetic reconnection is the most probable mechanism leading to the generation of the solar jets. For instance, such jets are really seen in soft X-ray images from *Yohkoh* (Shibata et al. 1992, 1994; Strong et al. 1992).

Aurass et al. (1994) reported on the first detection of correlated type III radio bursts and plasma jets in the corona by a comprehensive analysis of radio and soft X-ray data. Solar type III radio bursts are usually regarded as the signature of beams of supra-thermal electrons (Nelson & Melrose 1985). These electron beams excite high frequency plasma (e.g., Langmuir) waves, which convert into escaping radio waves by scattering at ion density fluctuations and/or by coalescence with other plasma waves. Thus, the radio emission takes place near the local electron plasma frequency $f_{\rm pe} = (e^2 N_{\rm e}/(\pi m_{\rm e}))^{1/2}$ (e, elementary charge; $N_{\rm e}$, electron number density; $m_{\rm e}$, electron mass) and/or its harmonics (Melrose 1985). Since the electron plasma frequency depends on the electron number density, the higher/lower frequencies are emitted in the lower/higher corona, respectively, due to the gravitational stratification of the solar atmosphere. An example of a solar type III radio burst is presented in Fig. 2. It shows a dynamic radio spectrum in the range 110–400 MHz. At first, a stripe of enhanced radio emission starts near 350 MHz at 08:18:51 UT and rapidly drifts towards lower frequencies down to 110 MHz. That is a typical type III radio burst, which is considered to be an electron beam traveling along open magnetic field lines outwards in the corona. Another feature started near 300 MHz at 08:18:53 UT reached 230 MHz at 08:18:57 UT and turned back towards higher frequencies. It reached 400 MHz at 08:19:00 UT. Such a feature is called a type U radio burst.

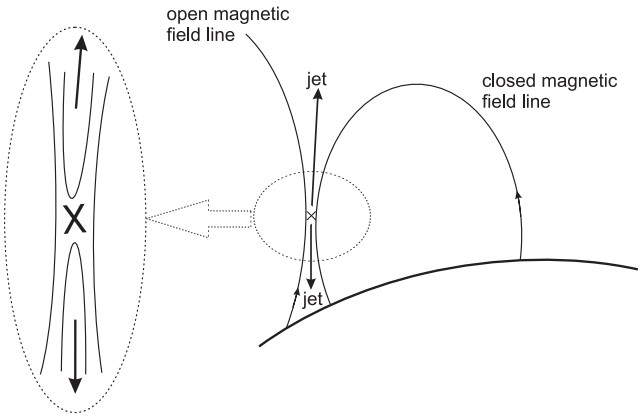

Fig. 1. Sketch of the magnetic field configuration possibly leading to reconnection and, subsequently, to the establishment of jets in the solar corona. The insert on the left-hand side shows an enlargement of the magnetic field lines at the reconnection site.

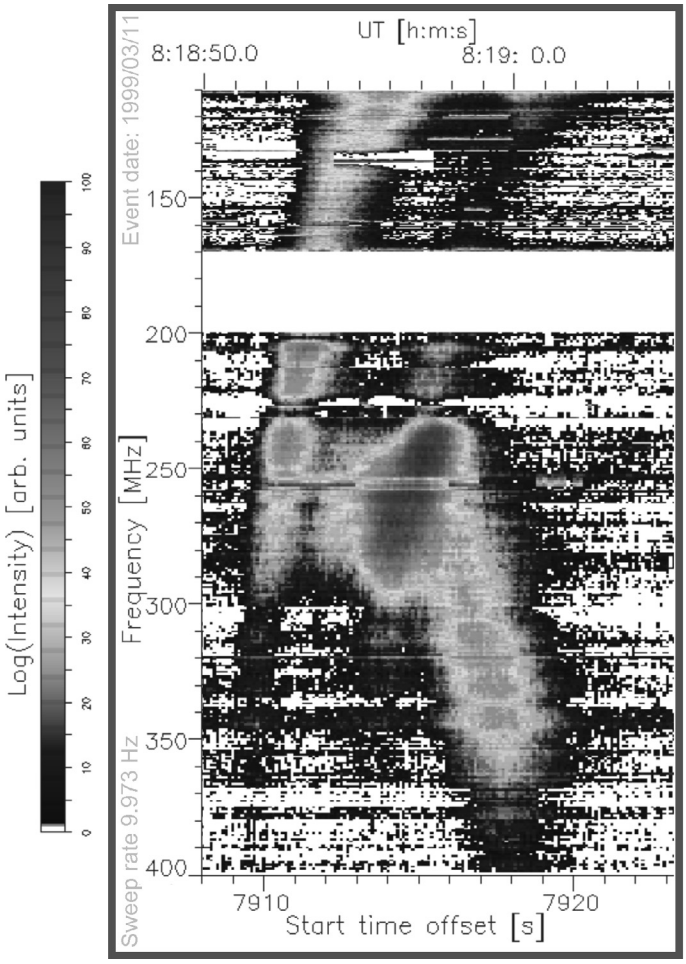

Fig. 2. Dynamic radio spectrum recorded by the radio spectralpolarimeter (Mann et al. 1992) of the Astrophysical Institute Potsdam in the frequency range 110–400 MHz. It shows an example of a solar type III and U radio bursts. Further explanations are given in Sect. 1.

According our interpretation, it should be considered as an electron beam traveling along closed magnetic field lines in the corona. The dynamic radio spectrogram indicates that both electron beams are generated near the same place and time in the corona.

Pick et al. (1994) presented a joint observation from the soft X-ray telescope (SXT) aboard *Yohkoh* and Nançay multifrequency radioheliograph. A type III/U radio burst has been used as a tracer of a coronal structure and its subsequent development. Kundu et al. (1994, 1995) looked for non-thermal radio emission at metric wavelengths from flaring solar X-ray bright points (XBPs) identified in *Yohkoh*/SXT data. Several type IIIs were clearly associated (temporal and spatial) with isolated flaring XBPs. The authors also noted a jet-like feature, which is well directed along the path of the electron beams responsible for the type III radio burst.

The association between metric type III bursts and soft X-ray jets has been summarized by Raulin et al. (1996). In this work, further evidence is presented for the production of non-thermal electrons associated with soft X-ray jets. The most important result is the finding that the centroids of the type III bursts at different frequencies are aligned in the direction of the soft X-ray jets. The authors conclude that the soft X-ray jets are probably the dense coronal structures along which the type III electron beams propagate.

The interaction of a hot neutral plasma stream (jet) with the surrounding plasma is studied in terms of a kinetic approach in the present paper. This interaction gives rise to the excitation of electrostatic fluctuations at which electrons can be energized. The dispersion relation of electrostatic waves is derived in a kinetic manner, i.e., from the Vlasov-Maxwell equations, in Sect. 2. The interaction of a hot jet with the coronal background plasma is studied in Sect. 3. In Sect. 4, the conditions of excitation of electrostatic fluctuations are discussed for the circumstances of the interaction of a jet with the surrounding background plasma. The movement of an electron in an oscillatory electrostatic field is investigated in Sect. 5. The results of the paper are summarized in Sect. 6.

2. Kinetic approach

A collisionless plasma can be described by the well-known Vlasov-Maxwell equations (see, e.g., Krall & Trivelpiece 1986; and Baumjohann & Treumann 1997). It is intended to study the interaction of a hot neutral plasma stream (jet) with the surrounding background plasma with the aim searching for plasma wave excitation. That is usually done by a linear treatment of the Vlasov-Maxwell equations leading to a homogeneous system of equations

$$\epsilon_{ij} E_j = 0 \tag{1}$$

with the dielectric tensor ϵ_{ij}. The determinant of the tensor ϵ_{ij} provides the dispersion relation of the different waves. Here, $\boldsymbol{E}$ denotes the vector of the electric field accompanied by these plasma waves. The jet and the waves are assumed to propagate along the ambient magnetic field. That is chosen to be the z-direction. Since it is intended to look for the excitation of electrostatic waves, the system of Eq. (1) can be reduced to

$$\epsilon_{33}\, E_z = 0 \tag{2}$$

with

$$\epsilon_{33} = 1 - 2\pi \sum_s \frac{\omega_{\mathrm{p}s}^2}{k^2} \int_{-\infty}^{\infty} \mathrm{d}V_\parallel \int_0^{\infty} \mathrm{d}V_\perp V_\perp \frac{k}{kV_\parallel - \omega} \frac{\partial f_s}{\partial V_\parallel} \tag{3}$$

with the wave number k and the frequency ω (Baumjohann & Treumann 1997). Here, each kind of particle s with the charge q_s, the mass m_s, the temperature T_s, and the velocity distribution function f_s interacts with each other by electromagnetic forces. N_s and $\omega_{\mathrm{p}s} = (4\pi q_s^2 N_s/m_s)^{1/2}$ denote the number density of each kind of particles and its corresponding plasma frequency, respectively.

Since a magnetized plasma is considered, the velocity distribution function f_s basically depends on the particle velocities parallel ($V_\parallel$) and perpendicular ($V_\perp$) to the ambient magnetic field, i.e., $f_s = f_s(V_\parallel, V_\perp)$. For the presented study, a drifting Maxwellian distribution is assumed for the velocity distribution function

$$f_s = \frac{1}{(2\pi v_{\mathrm{th},s}^2)^{3/2}}\, \mathrm{e}^{-[(V_\parallel - V_{0,s})^2 + V_\perp^2]/2v_{\mathrm{th},s}^2} \tag{4}$$

with $v_{\mathrm{th},s} = (k_\mathrm{B} T_s/m_s)^{1/2}$ as the thermal velocity of the particle species s, since the jet is regarded as propagating along the magnetic field lines. $V_{0,s}$ denotes the drift velocity of the species s. Inserting the velocity distribution function (4) into Eq. (3) and

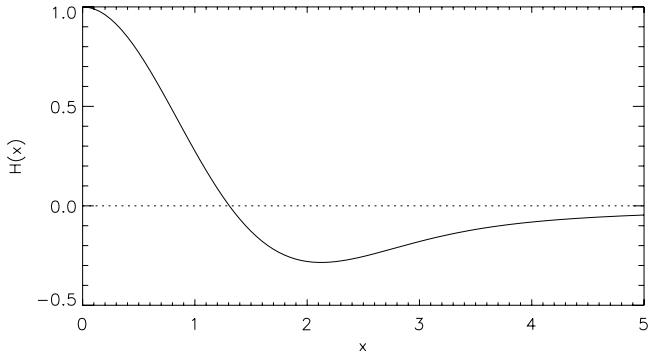

Fig. 3. Numerical behavior of the function $H(x)$.

performing the integrals, one gets the expression for the dispersion relation of electrostatic waves

$$-k^2 = \sum_s \frac{\omega_{\mathrm{ps}}^2}{v_{\mathrm{th},s}^2} H(\xi_s) \tag{5}$$

with $\xi_s = (V_{\mathrm{ph}} - V_{0,s})2^{-1/2}/v_{\mathrm{th},s}$. $V_{\mathrm{ph}} = \omega/k$ is the phase velocity. The function $H(x)$ is given by

$$H(x) = 1 + x\,Z(x) \tag{6}$$

with the well-defined plasma dispersion function

$$Z(x) = \frac{1}{\pi^{1/2}} \int_{-\infty}^{+\infty} \mathrm{d}u\, \frac{\mathrm{e}^{-u^2}}{u - x} \tag{7}$$

(Baumjohann & Treumann 1997). Figure 3 shows the numerical behavior of the $H(x)$-function. The H-function changes its sign at $x = 1.3$, takes a global minimum of -0.2875 at $x = 2.1$, and finally tends to zero for $x \to \infty$.

3. Jet plasma interaction

Now, the interaction of a hot plasma jet with the coronal background plasma is studied. Both, the background plasma and the jet are neutral. In the case of the background plasma the electrons and protons have the temperature T_0, and their drift velocity is zero. Then, its parameters can be fixed to be

$$\begin{aligned} V_{\mathrm{b0,e}} &= V_{\mathrm{b0,p}} = 0 \\ T_{\mathrm{b,e}} &= T_{\mathrm{b,p}} = T_0 \\ N_{\mathrm{b,e}} &= N_{\mathrm{b,p}} = (1-\nu)N_0. \end{aligned}$$

The jet is drifting with the velocity V_0 with respect to the background plasma. The electrons of the jet are considered to be hot, i.e., their temperature is θT_0 (with $\theta > 1$), whereas the protons of the jet have the same temperature as the protons of the background plasma. The number density of the jet electrons is νN_0, i.e., N_0 gives the total number density of all electrons in the combined jet–background plasma system. The same is valid for the protons since neutral plasma is considered. Finally, the parameters of the jet are given by

$$\begin{aligned} V_{\mathrm{j0,e}} &= V_{\mathrm{j0,p}} = V_0 \\ T_{\mathrm{j,e}} &= \theta T_0 \quad \text{and} \quad T_{\mathrm{j,p}} = T_0 \\ N_{\mathrm{j,e}} &= N_{\mathrm{j,p}} = \nu N_0. \end{aligned}$$

Here, the indices e, p, b, and j are abbreviations for the electrons, the protons, the background plasma, and the jet, respectively.

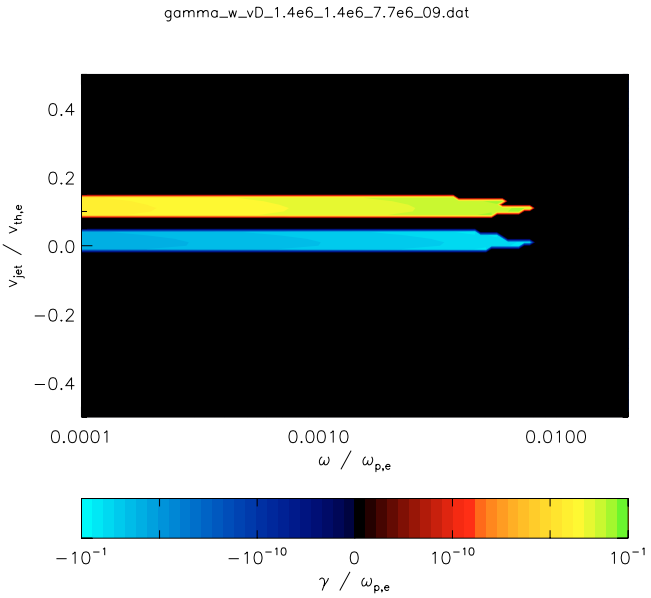

Fig. 4. Results of the numerical evaluation of Eq. (8) for choosing $\nu = 0.9$ and $\theta = 5.5$. The growth rate γ is presented in its dependence on the wave frequency ω and jet speed $v_{\mathrm{jet}}/v_{\mathrm{th,e}}$.

Thus, the considered plasma represents a four component plasma. Then, the dispersion relation of Eq. (5) reduces to

$$\begin{aligned} -q^2 &= (1-\nu)H(\xi_{\mathrm{b,e}}) + (1-\nu)H(\xi_{\mathrm{b,p}}) \\ &\quad + \frac{\nu}{\theta} H(\xi_{\mathrm{j,e}}) + \nu H(\xi_{\mathrm{j,p}}) \end{aligned} \tag{8}$$

with $\xi_{\mathrm{b,e}} = v_{\mathrm{ph}}/2^{1/2}$, $\xi_{\mathrm{b,p}} = v_{\mathrm{ph}}/(2\mu_{\mathrm{e}})^{1/2}$, $\xi_{\mathrm{j,e}} = (v_{\mathrm{ph}} - v_0)/(2\theta)^{1/2}$, and $\xi_{\mathrm{j,p}} = (v_{\mathrm{ph}} - v_0)/(2\mu_{\mathrm{e}})^{1/2}$ ($\mu_{\mathrm{e}} = m_{\mathrm{e}}/m_{\mathrm{p}}$; m_{p}, proton mass). Here, the frequency ω, the wave number k, the phase velocity V_{ph}, and the drift velocity V_0 are normalized to the plasma frequency $\omega_{\mathrm{p0}} = (4\pi e^2 N_0/m_{\mathrm{e}})^{1/2}$, the Debye length $\lambda_{\mathrm{De}} = v_{\mathrm{th,e}}/\omega_{\mathrm{p0}}$, and the thermal electron speed $v_{\mathrm{th,e}} = (k_{\mathrm{B}} T_0/m_{\mathrm{e}})^{1/2}$, respectively, ($k_{\mathrm{B}}$, Boltzmann's constant). Here the quantities $q = k\,v_{\mathrm{th,e}}/\omega_{\mathrm{p0}}$, $v_{\mathrm{ph}} = V_{\mathrm{ph}}/v_{\mathrm{th,e}}$ and $v_0 = V_0/v_{\mathrm{th,e}}$ are already normalized ones.

To discuss under which conditions a wave-like solution of Eq. (8), i.e., $q^2 > 0$, is obtained, the conditions under which the right hand becomes negative must be evaluated. Since the jet speeds are in the range 10–1000 km s^{-1} (Shimojo et al. 1996) and the thermal electron velocity is 4600 km s^{-1} for a coronal temperature of 1.4×10^6 K, $v_0 \ll 1$. Therefore, the waves excited by the jet plasma interaction have phase speeds with $v_{\mathrm{ph}} \ll 1$. That leads to $\xi_{\mathrm{b,e}}, \xi_{\mathrm{j,e}} \ll 1$ and, consequently, to $H(\xi_{\mathrm{b,e}}) \approx 1$ and $H(\xi_{\mathrm{j,e}}) \approx 1$. The H-function (see Eq. (6)) has a global minimum of -0.2875 (see Fig. 3) at $x = 2.1$. If the jet speed is adjusted in such a way that the H-function takes its minimum, a wave-like solution of Eq. (8), i.e., $q^2 > 0$, appears necessary, if $(1-\nu) + (\nu/\theta) < 0.2875$ and hence $\nu > 0.7125/[1 - 1/\theta]$. This condition should be fulfilled in the sense of a rough estimate, i.e., at least $\theta \geq 3.4783$ (for $\nu \leq 1$). From observations (see Shimojo 1999; Shimojo & Shibata 2000), one could estimate the upper temperature limit of the jet, i.e., $\theta \leq 5.71$ (which leads to $\nu \geq 0.864$). In conclusion, only a jet with hot electrons is able to provide a wave-like solution of Eq. (8).

For discussing the jet plasma interaction, the jet parameters observed during the solar event on December 28, 1993 (Shimojo 1999, p. 66) are adopted for a careful numerical evaluation of Eq. (8). At this event the jet had a speed of 532 km s^{-1} (=0.12$v_{\mathrm{th,e}}$ with $v_{\mathrm{th,e}} = 4\,600$ km s^{-1} for a coronal temperature of $1.4{\times}10^6$ K)

and a temperature of $7.4–8.2 \times 10^6$ K (i.e., $\theta = 5.5$). Choosing $\nu = 0.9$ and $\theta = 5.5$ for the parameters, the numerical evaluation of Eq. (8) provides an instability for jet speeds in the interval $0.09 < v_0 < 0.15$, i.e., in the range 415–690 km s^{-1} (Fig. 4), leading to an excitation of electrostatic waves up to frequencies of $0.01\,\omega_{p0}$. These waves are of the ion-acoustic mode (Baumjohann & Treumann 1997). The maximum of the growth rate $\gamma_{max} = 0.00319\,\omega_{p0}$ appears at a frequency $\omega = 0.00372\,\omega_{p0}$ (Fig. 4). In summary, the interaction of the jet with the background plasma leads to an instability for a small range of jet speeds, i.e., 415–690 km s^{-1}, exciting electrostatic waves in the sense of the ion-acoustic mode. The appearance of the instability requires hot electrons in the jet.

4. Movement of electrons in oscillatory electrostatic field

The equation of motion of an electron considered to be a test particle in an electrostatic field is usually given by

$$\frac{\mathrm{d}p}{\mathrm{d}t} = -eE = e\frac{\partial\varphi}{\partial x}, \tag{9}$$

with the electrostatic potential φ, the momentum $p = m_e v/(1-\beta^2)^{1/2}$, and particle velocity v ($\beta = v/c$; c, velocity of light). Introducing dimensionless quantities, the equation of motion is transformed into the normalized one:

$$\frac{1}{\beta_{th}}\,\frac{1}{(1-\beta^2)^{3/2}}\,\frac{\mathrm{d}\beta}{\mathrm{d}t} = \frac{\partial\phi}{\partial x}, \tag{10}$$

with $\beta_{th} = V_{th,e}/c$. In Eq. (9), the time t, the spatial coordinate x, and the electrostatic potential φ are normalized to the inverse of the electron plasma frequency ω_{p0}^{-1}, the Debye-length $v_{th,e}/\omega_{p0}$, and $k_B T_0/e$, i.e., $\phi = e\varphi/k_B T_0$, respectively. Additionally, the definition of the velocity $v = \mathrm{d}x/\mathrm{d}t$, i.e.,

$$\frac{\mathrm{d}x}{\mathrm{d}t} = \frac{\beta}{\beta_{th}} \tag{11}$$

in normalized quantities, must be introduced to the system of equations for describing the test particle motion. The ansatz

$$\phi = \phi_0\,\mathrm{e}^{\gamma t}\cos\left[q\,x(t) - \omega\,t\right] \tag{12}$$

is adopted for the spatial–temporal behavior of the electrostatic potential. Here, the same normalization has been employed. The electrostatic fluctuations are generated by the instability appearing due to the jet plasma interaction (see Sect. 3). Since the conditions of maximum growth rate should be used, $\gamma = 0.00319$, $\omega = 0.00372$, and $q = 0.05$ are chosen. At the thermal, i.e., undisturbed level, the amplitude of the electrostatic (ion-acoustic) fluctuations can be assumed to be about $k_B T$, i.e., $\phi_0 = 1$. The normalized equations of motion (Eqs. (10) and (11)) have been numerically solved with the choice of these parameters. Since the electron is regarded as a test particle, it must be collisionless with respect to Coulomb collisions. To be sure concerning this subject, the initial velocity of the electron is chosen to be 4 times the thermal one, i.e., $\beta_0 = 0.0613$ with a thermal electron velocity of 4600 km s^{-1}. It corresponds to a kinetic energy of about 1 keV. In summary, the initial conditions are $x(t=0) = 0$ and $\dot{x}(t=0) = 4$ in the sense of normalized quantities. The resulted movement in the x–t plane is presented in Fig. 5.

As seen in Fig. 5, the electron is initially moving with a nearly constant velocity until $t \approx 650$ in the initial phase. Then,

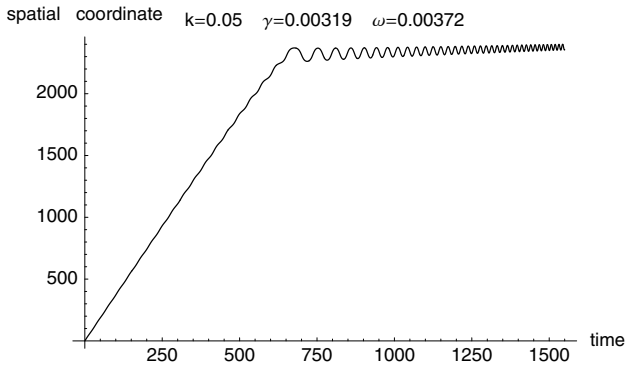

Fig. 5. Spatial movement of the test electron in the x–t plane for $q = 0.05$, $\gamma = 0.00319$, and $\omega = 0.00372$.

its motion is dramatically changed into a much more slower one superimposed by an oscillatory motion with a frequency increasing with time. That can be explained in the following manner: initially, the amplitude of the electrostatic wave (see Eq. (12)) wave is small, so that its influence on the electron motion can be neglected. Then, the electron homogeneously propagates with a constant velocity of β_0. Since the amplitude of the electrostatic field is increasing with time t, its influence on the particle motion will become essential, if the potential energy of the particle in the electrostatic wave is comparable with the kinetic energy of the particle, i.e.,

$$\frac{W}{k_B T_0} = \frac{1}{\beta_{th}^2}\left[\frac{1}{\sqrt{1-\beta^2}} - 1\right] = \phi_0\,\mathrm{e}^{\gamma t}. \tag{13}$$

That state is reached after the time

$$t_b = \frac{1}{\gamma}\,\ln\left(\frac{W_0}{k_B T_0}\cdot\frac{1}{\phi_0}\right). \tag{14}$$

One gets $t_b = 652$ for $W_0/k_B T = 8$ corresponding to $\beta_0 = 4\,V_{th,e}/c = 0.0613$ ($k_B T_0 = 0.12$ keV for $T_0 = 1.4 \times 10^6$ K), as can be seen in Fig. 5. After this time the electrostatic field dramatically changes the particle movement. Namely, the particle co-moves with the electrostatic wave, i.e., its averaged velocity is the phase speed of the wave, as depicted in Fig. 5. An oscillatory motion with temporally increasing frequency is superimposed upon this slow co-motion with the wave. That can be demonstrated in the following way: Inserting the ansatz (12) into Eq. (10) one gets

$$\frac{1}{\beta_{th}}\,\frac{\mathrm{d}\beta}{\mathrm{d}t} = -q\,\phi_0\,\mathrm{e}^{\gamma t}\,\sin\left[q\,x(t) - \omega t\right] \tag{15}$$

in the non-relativistic approach (i.e., $\beta \ll 1$). In the case of the co-motion with the wave, the function $x(t)$ can be expressed by

$$x(t) = v_{ph}^{*} t + \delta x + x_0 \tag{16}$$

with $v_{ph}^{*} = \omega/q$ as the phase velocity of the wave, Here, δx represents the oscillatory motion superimposed on the slowly translatory motion. Inserting the expression (16) into Eq. (15) and using Eq. (11) one obtains

$$\frac{\mathrm{d}^2\delta x}{\mathrm{d}t^2} = -q\phi_0\,\mathrm{e}^{\gamma t}\,\sin\left[q\,\delta x + q\,x_0\right]. \tag{17}$$

Since the oscillatory motion has small amplitudes, $q\,\delta x \ll 1$ should be assumed. Then, Eq. (17) reduces to

$$\frac{\mathrm{d}^2\delta x}{\mathrm{d}t^2} + \varpi^2\delta x = -q\,\phi_0\,\mathrm{e}^{\gamma t}\,\sin\left[q x_0\right] \tag{18}$$

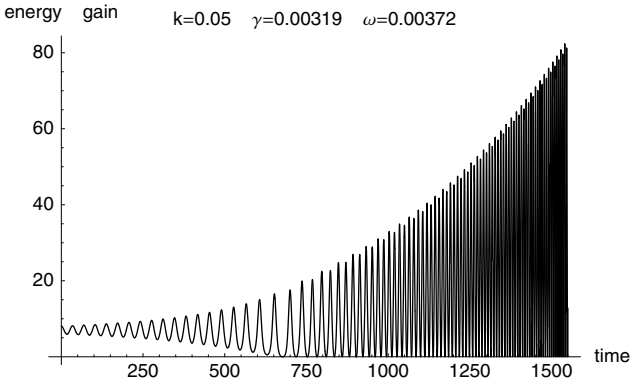

Fig. 6. Energy gain of the test electron with the time during the movement for $q = 0.05$, $\gamma = 0.00319$, and $\omega = 0.00372$.

with $\varpi^2 = q^2\phi_0 \exp(\gamma t)\cos[qx_0]$. Equation (18) actually represents an equation of an oscillatory motion with the frequency ϖ, which increases with time. That can be really observed in Fig. 5. (For instance, x_0 can be adjusted in such a way that $\sin[qx_0] = 0$.) Adopting the parameters used in the numerical solution of the Eqs. (10) and (11), one finds a period of $2\pi/\varpi = 35$ at $t = 800$ for the oscillatory motion. This value is similar to that deduced from the numerical calculations as depicted in Fig. 5. It should be emphasized that a total agreement between the analytical approach and the numerical solution should not be expected since the numerical result (Fig. 5) is the exact one, whereas the analytical treatment presented above is only an approximative approach. It, however, demonstrates the appearance of an oscillatory motion with a temporally increasing frequency during the co-motion with the wave.

While co-moving with the wave, the electron gets energy from the electrostatic wave (Fig. 6). Figure 6 shows that the particle gets an energy of 80 $k_B T_0$ within a period of $\approx 1600/\omega_{p0}$, i.e., the electron obtains an energy of 10 keV within 0.85 μs for $\omega_{p0} = 2\pi \times 300$ MHz, for instance. The value of 300 MHz has been chosen for this example, since type III radio bursts associated with jets usually appear at this frequency level (see, e.g., Fig. 1).

5. Discussion

During magnetic reconnection, which is the basic process of solar flares, jets of hot plasma are ejected from the reconnection site into the surrounding coronal plasma. The interaction of such jets with background plasma leads to the excitation of electrostatic waves due to an instability if the jet speed is in the range 415−690 km s^{-1}. Such values are typical ones for jets as observed in the soft X-ray images by *Yohkoh* (Shimojo et al. 1996; Shimojo & Shibata 2000).

If the jet penetrates into the surrounding coronal plasma, it is decelerated due to Coulomb collisions within a period of the order of the Coulomb collision time t_{Cc}, which is given by

$$t_{Cc} = \frac{1}{\omega_{pe}} \frac{4\pi\lambda_{De}^3 N_e}{\ln\Lambda} \tag{19}$$

with $\Lambda = 4\pi\lambda_{De}^3 N_0$ (Estel & Mann 1999). At the 300 MHz level and a coronal temperature of 1.4×10^6 K, one gets $N_0 = 1.12 \times 10^9$ cm^{-3} and $\lambda_{De} = 0.244$ cm resulting in $t_{Cc} = 10^7/\omega_{p0}$. In comparison, the growing time $t_{growing}$ for the excitation of electrostatic waves is given by $t_{growing} = \gamma^{-1}/\omega_{p0} = 313/\omega_{p0}$ for $\gamma = 0.00319$. Thus, the instability acts much faster than the deceleration of the jet due to Coulomb collisions.

As discussed in this paper, the plasma stream ejected from the reconnection site passes through the surrounding coronal plasma leading to the excitation of electrostatic fluctuations in terms of the ion-acoustic mode. If these fluctuations act on supra-thermal electrons, these electrons co-move with the wave (Fig. 5) and gain energy (Fig. 6). That process represents a collisionless energizing and/or heating of the electrons during flares. It is well-known that electrons are rapidly heated in a collisionless manner during flares. That is impressively seen in the hard X-ray emission of the flaring plasma as observed by the spacecraft RHESSI, for instance.

Since the instability only appears in a small range of the jet speed (Fig. 4), the enhanced level of electrostatic fluctuations is localized in a small spatial region in the corona. Consequently, if the energized electrons leave the region of instability, some of them can run away with a high velocity along a magnetic field line. That leads to either solar type III or type U radio bursts during their propagation along open and closed magnetic field lines (see Fig. 1 for example), respectively.

The observations show that there are generally three kinds of events (Aurass et al. 1994; Pick et al. 1994; Raulin et al. 1996):

i. jets that are not accompanied by type III bursts;
ii. jets with a simultaneous appearance of type III bursts;
iii. jets accompanied with type III bursts, but with a temporal delay concerning the jet onset time.

They can be explained in the framework of our approach. Since the instability only occurs in a small range of the jet speed around V_0, jets with a speed smaller than V_0 do not give rise to an electrostatic instability and, hence, to type III bursts (case i). On the other hand, if the jet speed is greater than V_0, it is initially not able to excite electrostatic fluctuations. However, the jet is decelerating due to its interaction with the surrounding plasma, e.g., due to Coulomb collisions. Then, it needs time until the jet speed slows down to V_0 leading to the onset of the electrostatic instability and, consequently, to the occurrence of type III radio bursts (case iii). That could be the reason of the observed delay between the onset of the jet and that of the type III burst (Aurass et al. 1994). Only in the special case, at which the jet speed is very close to V_0, can the type III radio bursts simultaneously appear with the jet (case ii). In summary, the interaction of a solar jet ejected from the reconnection site with the surrounding plasma leads to both the collisionless energizing and/or heating of electrons (as seen in the hard X-ray emission) and to type III bursts (as observed in the solar radio emission during flares). Here, the kinetic energy of the jet is partly transfered into energy of electrostatic fluctuations and, subsequently, into the energy of the electrons.

Acknowledgements. The authors thank to Germar Rausche and Hakan Önel for helpful and stimulating discussions. RM was financially supported by Deutscher Akademisher Austauschdienst (DAAD) grant Ref. 324 A/03/10336.

References

Aurass, H., Klein, K.-L., & Martens, P. C. H. 1994, Sol. Phys., 155, 203
Baumjohann, W., & Treumann R. A. 1997, Basic Space Plasma Physics (London: Imperial College Press)
Estel, C., & Mann, G. 1999, A&A, 345, 276
Heyvaerts, J. 1981, in Solar Flare Magnetohydrodynamics, ed. E. R. Priest (Gordon and Breach Science Publishers), Ch. 8
Krall, N. A., & Trivelpiece, A. W. 1986, Principles of Plasma Physics (San Francisco Press)

Kundu, M. R., Strong, K. T., Pick, M., et al. 1994, in Proc. Kofu Symposium, ed. S. Enome, & T. Hirayama, NRO Rep., 360, 343
Kundu, M. R., Raulin, J. P., Nitta, N., et al. 1995, ApJ, 447, L135
Mann G., Aurass, H., Voigt, W., & Paschke, J. 1992, in Proc. First SOHO Workshop, ESA SP-446, 447
Melrose, D. B. 1985, in Solar Radiophysics, ed. D. J. McLean, & N. R. Labrum (Cambridge: Cambridge University Press), Chs. 8, 9
Nelson, G. J., & Melrose, D. B. 1985, in Solar Radiophysics, ed. D. J. McLean, & N. R. Labrum (Cambridge: Cambridge University Press), Ch. 13
Pick, M., Raoult, A., Trottet, G., et al. 1994, in Proc. Kofu Symposium, ed. S. Enome, & T. Hirayama, NRO Rep., 360, 263
Raulin, J. P., Kundu, M. R., Hudson, H. S., Nitta, N., & Raoult, A. 1996, A&A, 306, 299
Shibata, K., Ishido, Y., Acton, L. W., et al. 1992, PASJ, 44, L173
Shibata, K., Yokoyama, T., & Shimojo, M. 1994, in Proc. Kofu Symposium, ed. S. Enome, & T. Hirayama, NRO Rep., 360, 75
Shimojo, M. 1999, Studies of Solar Coronal X-ray Jets, Ph.D. Thesis, Graduate University for Advance Studies, Japan
Shimojo, M., & Shibata, K. 2000, ApJ, 542, 1100
Shimojo, M., Hashimoto, S., Shibata, K., et al. 1996, PASJ, 48, 123
Strong, K. T., Harvey, K, Hirayama, T., et al. 1992, PASJ, 44, L161
Treumann R. A., & Baumjohann, W. 1997, Advanced Space Plasma Physics (London: Imperial College Press)
Yokoyama, T., & Shibata, K. 1994, in Proc. Kofu Symposium, ed. S. Enome, & T. Hirayama, NRO Rep., 360, 367
Yokoyama, T., & Shibata, K. 1995, Nature, 375, 42